

Evidence for $B \rightarrow \eta' \pi$ and Improved Measurements for $B \rightarrow \eta' K$

J. Schümann,²² C. H. Wang,²² K. Abe,⁷ I. Adachi,⁷ H. Aihara,⁴³ D. Anipko,¹ K. Arinstein,¹ Y. Asano,⁴⁷ T. Aushev,¹¹ A. M. Bakich,³⁸ V. Balagura,¹¹ E. Barberio,¹⁸ M. Barbero,⁶ A. Bay,¹⁶ I. Bedny,¹ U. Bitenc,¹² I. Bizjak,¹² S. Blyth,²¹ A. Bondar,¹ A. Bozek,²⁴ M. Bračko,^{7,17,12} T. E. Browder,⁶ M.-C. Chang,⁴² P. Chang,²³ Y. Chao,²³ A. Chen,²¹ W. T. Chen,²¹ B. G. Cheon,³ Y. Choi,³⁷ Y. K. Choi,³⁷ A. Chuvikov,³² S. Cole,³⁸ J. Dalseno,¹⁸ M. Danilov,¹¹ M. Dash,⁴⁸ J. Dragic,⁷ A. Drutskoy,⁴ S. Eidelman,¹ D. Epifanov,¹ S. Fratina,¹² N. Gabyshev,¹ T. Gershon,⁷ A. Go,²¹ G. Gokhroo,³⁹ B. Golob,^{50,12} A. Gorišek,¹² H. C. Ha,¹⁴ J. Haba,⁷ T. Hara,²⁹ N. C. Hastings,⁴³ K. Hayasaka,¹⁹ H. Hayashii,²⁰ M. Hazumi,⁷ L. Hinz,¹⁶ T. Hokuue,¹⁹ Y. Hoshi,⁴¹ S. Hou,²¹ W.-S. Hou,²³ Y. B. Hsiung,²³ T. Iijima,¹⁹ A. Imoto,²⁰ K. Inami,¹⁹ A. Ishikawa,⁷ R. Itoh,⁷ M. Iwasaki,⁴³ Y. Iwasaki,⁷ J. H. Kang,⁴⁹ P. Kapusta,²⁴ N. Katayama,⁷ H. Kawai,² T. Kawasaki,²⁶ H. R. Khan,⁴⁴ H. Kichimi,⁷ S. K. Kim,³⁶ S. M. Kim,³⁷ K. Kinoshita,⁴ R. Kulasiri,⁴ R. Kumar,³⁰ C. C. Kuo,²¹ A. Kuzmin,¹ Y.-J. Kwon,⁴⁹ J. S. Lange,⁵ J. Lee,³⁶ T. Lesiak,²⁴ A. Limosani,⁷ D. Liventsev,¹¹ J. MacNaughton,⁹ G. Majumder,³⁹ F. Mandl,⁹ D. Marlow,³² T. Matsumoto,⁴⁵ A. Matyja,²⁴ W. Mitaroff,⁹ H. Miyake,²⁹ H. Miyata,²⁶ Y. Miyazaki,¹⁹ R. Mizuk,¹¹ G. R. Moloney,¹⁸ T. Mori,⁴⁴ T. Nagamine,⁴² I. Nakamura,⁷ E. Nakano,²⁸ M. Nakao,⁷ Z. Natkaniec,²⁴ S. Nishida,⁷ O. Nitoh,⁴⁶ S. Ogawa,⁴⁰ T. Ohshima,¹⁹ T. Okabe,¹⁹ S. Okuno,¹³ S. L. Olsen,⁶ H. Ozaki,⁷ P. Pakhlov,¹¹ H. Palka,²⁴ C. W. Park,³⁷ H. Park,¹⁵ N. Parslow,³⁸ L. S. Peak,³⁸ R. Pestotnik,¹² L. E. Piilonen,⁴⁸ M. Rozanska,²⁴ Y. Sakai,⁷ T. R. Sarangi,⁷ N. Sato,¹⁹ T. Schietinger,¹⁶ O. Schneider,¹⁶ C. Schwanda,⁹ R. Seidl,³³ K. Senyo,¹⁹ M. E. Sevier,¹⁸ M. Shapkin,¹⁰ H. Shibuya,⁴⁰ B. Shwartz,¹ V. Sidorov,¹ A. Sokolov,¹⁰ A. Somov,⁴ N. Soni,³⁰ R. Stamen,⁷ S. Stanič,²⁷ M. Starič,¹² K. Sumisawa,²⁹ S. Suzuki,³⁴ F. Takasaki,⁷ K. Tamai,⁷ N. Tamura,²⁶ M. Tanaka,⁷ G. N. Taylor,¹⁸ Y. Teramoto,²⁸ X. C. Tian,³¹ K. Trabelsi,⁶ T. Tsuboyama,⁷ T. Tsukamoto,⁷ S. Uehara,⁷ T. Uglov,¹¹ K. Ueno,²³ S. Uno,⁷ P. Urquijo,¹⁸ Y. Usov,¹ G. Varner,⁶ K. E. Varvell,³⁸ S. Villa,¹⁶ C. C. Wang,²³ M.-Z. Wang,²³ Y. Watanabe,⁴⁴ E. Won,¹⁴ Q. L. Xie,⁸ A. Yamaguchi,⁴² Y. Yamashita,²⁵ M. Yamauchi,⁷ J. Ying,³¹ Y. Yusa,⁴² C. C. Zhang,⁸ L. M. Zhang,³⁵ Z. P. Zhang,³⁵ V. Zhilich,¹ and D. Zürcher¹⁶

(Belle Collaboration)

¹*Budker Institute of Nuclear Physics, Novosibirsk*

²*Chiba University, Chiba*

³*Chonnam National University, Kwangju*

⁴*University of Cincinnati, Cincinnati, Ohio 45221*

⁵*University of Frankfurt, Frankfurt*

⁶*University of Hawaii, Honolulu, Hawaii 96822*

⁷*High Energy Accelerator Research Organization (KEK), Tsukuba*

⁸*Institute of High Energy Physics, Chinese Academy of Sciences, Beijing*

⁹*Institute of High Energy Physics, Vienna*

¹⁰*Institute of High Energy Physics, Protvino*

¹¹*Institute for Theoretical and Experimental Physics, Moscow*

¹²*J. Stefan Institute, Ljubljana*

¹³*Kanagawa University, Yokohama*

¹⁴*Korea University, Seoul*

¹⁵*Kyungpook National University, Taegu*

¹⁶*Swiss Federal Institute of Technology of Lausanne, EPFL, Lausanne*

¹⁷*University of Maribor, Maribor*

¹⁸*University of Melbourne, Victoria*

¹⁹*Nagoya University, Nagoya*

²⁰*Nara Women's University, Nara*

²¹*National Central University, Chung-li*

²²*National United University, Miao Li*

²³*Department of Physics, National Taiwan University, Taipei*

²⁴*H. Niewodniczanski Institute of Nuclear Physics, Krakow*

²⁵*Nippon Dental University, Niigata*

²⁶*Niigata University, Niigata*

²⁷*Nova Gorica Polytechnic, Nova Gorica*

²⁸*Osaka City University, Osaka*

²⁹*Osaka University, Osaka*

³⁰*Panjab University, Chandigarh*³¹*Peking University, Beijing*³²*Princeton University, Princeton, New Jersey 08544*³³*RIKEN BNL Research Center, Upton, New York 11973*³⁴*Saga University, Saga*³⁵*University of Science and Technology of China, Hefei*³⁶*Seoul National University, Seoul*³⁷*Sungkyunkwan University, Suwon*³⁸*University of Sydney, Sydney NSW*³⁹*Tata Institute of Fundamental Research, Bombay*⁴⁰*Toho University, Funabashi*⁴¹*Tohoku Gakuin University, Tagajo*⁴²*Tohoku University, Sendai*⁴³*Department of Physics, University of Tokyo, Tokyo*⁴⁴*Tokyo Institute of Technology, Tokyo*⁴⁵*Tokyo Metropolitan University, Tokyo*⁴⁶*Tokyo University of Agriculture and Technology, Tokyo*⁴⁷*University of Tsukuba, Tsukuba*⁴⁸*Virginia Polytechnic Institute and State University, Blacksburg, Virginia 24061*⁴⁹*Yonsei University, Seoul*⁵⁰*University of Ljubljana, Ljubljana*

(Received 1 March 2006; published 10 August 2006)

We report evidence for the exclusive two-body charmless hadronic B meson decay $B \rightarrow \eta' \pi$, and improved measurements of $B \rightarrow \eta' K$. The results are obtained from a data sample of 386×10^6 $B\bar{B}$ pairs collected at the $Y(4S)$ resonance, with the Belle detector at the KEKB asymmetric-energy e^+e^- collider. We measure $\mathcal{B}(B^+ \rightarrow \eta' \pi^+) = [1.76_{-0.67}^{+0.67}(\text{stat})_{-0.14}^{+0.15}(\text{syst})] \times 10^{-6}$ and $\mathcal{B}(B^0 \rightarrow \eta' \pi^0) = [2.79_{-0.96}^{+1.02}(\text{stat})_{-0.34}^{+0.25}(\text{syst})] \times 10^{-6}$. We also find the ratio of $\frac{\mathcal{B}(B^+ \rightarrow \eta' \pi^+)}{\mathcal{B}(B^0 \rightarrow \eta' K^0)} = 1.17 \pm 0.08(\text{stat}) \pm 0.03(\text{syst})$ and measure the direct CP asymmetries for the charged modes.

DOI: [10.1103/PhysRevLett.97.061802](https://doi.org/10.1103/PhysRevLett.97.061802)

PACS numbers: 13.25.Hw, 11.30.Er, 11.30.Hv, 14.40.Nd

Information on the two-body charmless hadronic B meson decays $B \rightarrow \eta' \pi$ are incomplete at present [1]. Measurements of these decay modes can improve the understanding of the flavor-singlet penguin amplitude with intermediate t , c , and u quarks [2]. Furthermore, measurement of branching fractions for $B \rightarrow \eta' \pi$ decays can improve estimates of the expected standard model (SM) deviations of effective $\sin(2\phi_1)$ values in $b \rightarrow s$ modes from the value measured in $b \rightarrow c\bar{c}s$ decays [3]. Theoretical predictions for the branching fractions cover the ranges $(1-17) \times 10^{-6}$ and $(0.2-8) \times 10^{-6}$ for the charged and neutral decays, respectively [2,4,5]. Recently, the charged decay was measured by BABAR [6]. In contrast, the channels $B \rightarrow \eta' K$ have been precisely measured [7-9]. In the SM the decay $B \rightarrow \eta' K$ is believed to proceed dominantly via gluonic penguin processes [10], and has been evaluated with various QCD factorization and gluon anomaly approaches [11-15]. The measured branching fractions are, however, larger than the early expectations. This has led to speculations that SU(3)-singlet couplings unique to the η' meson or new physics [16] contribute to the amplitude. More precise measurements, in particular, for $B \rightarrow \eta' \pi$ are needed to constrain the amplitudes and to distinguish between theoretical models.

Additional constraints can be provided by the direct CP asymmetry, $A_{CP} = \frac{\mathcal{B}(\bar{B} \rightarrow \bar{f}) - \mathcal{B}(B \rightarrow f)}{\mathcal{B}(\bar{B} \rightarrow f) + \mathcal{B}(B \rightarrow f)}$, where f is the final

state and \bar{f} is its CP conjugate. Direct CP violation in the $B^+ \rightarrow \eta' \pi^+$ mode can be large in the SM [4], while a nonzero value for A_{CP} in $B^+ \rightarrow \eta' K^+$ may indicate a new physics contribution [10].

In this Letter, we report evidence for the decays $B \rightarrow \eta' \pi$, improved measurements of the $B \rightarrow \eta' K$ branching fractions, and the search for direct CP violation in the charged B -meson decay modes. The results are based on a data sample that contains 386×10^6 $B\bar{B}$ pairs, which is 35 times larger than our previous data set [8], collected with the Belle detector at the KEKB asymmetric-energy e^+e^- (3.5 on 8 GeV) collider [17]. KEKB operates at the $Y(4S)$ resonance ($\sqrt{s} = 10.58$ GeV).

The Belle detector is a large-solid-angle magnetic spectrometer that consists of a silicon vertex detector, a 50-layer central drift chamber (CDC), an array of aerogel threshold Čerenkov counters (ACC), a barrel-like arrangement of time-of-flight scintillation counters (TOF), and an electromagnetic calorimeter comprised of CsI(Tl) crystals located inside a superconducting solenoid coil that provides a 1.5 T magnetic field. An iron flux return located outside of the coil is instrumented to detect K_L^0 mesons and to identify muons. The detector is described in detail elsewhere [18]. Two inner detector configurations are used. A 2.0 cm beam pipe and a 3-layer silicon vertex detector are used for the first sample of 152×10^6 $B\bar{B}$ pairs (Set I),

while a 1.5 cm beam pipe, a 4-layer silicon detector, and a small-cell inner drift chamber are used to record the remaining 234×10^6 $B\bar{B}$ pairs (Set II) [19].

Charged hadrons are identified by combining information from the CDC (dE/dx), ACC, and TOF systems. Both kaons and pions are selected with an average efficiency of 86%. Tighter criteria are applied to the pion candidate in $B^+ \rightarrow \eta' \pi^+$, resulting in an average efficiency (kaon misidentification probability) of 77% (4%).

The η' mesons are reconstructed in the decays $\eta' \rightarrow \eta \pi^+ \pi^-$ (with $\eta \rightarrow \gamma\gamma$) and $\eta' \rightarrow \rho^0 \gamma$. We reconstruct π^0 , ρ^0 , η , η' , and K_S^0 candidates using the mass windows given in Table I. Photons originating from π^0 and η decays are required to have an energy of at least 50 MeV, and photons from η' in $\eta' \rightarrow \rho^0 \gamma$ of at least 100 MeV. The momenta of the π^\pm for ρ^0 candidates transverse to the beam line have to be greater than 200 MeV/ c , suppressing 60% of the background. The vertex of the $K_S^0 \rightarrow \pi^+ \pi^-$ has to be displaced from the interaction point and the K_S^0 momentum direction must be consistent with its flight direction [for a detailed description, see [20]]. For $B^0 \rightarrow \eta' \pi^0$, we require $|h_{\pi^0}| = \left| \frac{E(\gamma_1) - E(\gamma_2)}{E(\gamma_1) + E(\gamma_2)} \right| < 0.95(0.6)$ for $\eta' \rightarrow \eta \pi^+ \pi^-$ ($\eta' \rightarrow \rho^0 \gamma$), where $E(\gamma_{1,2})$ is the energy of the two π^0 decay photons. Similarly, we require $|h_\eta| < 0.85$. For combinatorial background arising from low energy photons $|h|$ peaks at 1.

B meson candidates are formed by combining an η' meson with a pion or a kaon candidate. Two kinematic variables are used to extract the B meson signal: the energy difference, $\Delta E = E_B - E_{\text{beam}}$, and the beam-energy constrained mass, $M_{\text{bc}} = \sqrt{E_{\text{beam}}^2/c^4 - (P_B/c)^2}$, where E_{beam} is the beam energy and E_B and P_B are the reconstructed energy and momentum of the B candidate. Events satisfying the requirements $M_{\text{bc}} > 5.22$ GeV/ c^2 and $|\Delta E| < 0.25$ GeV are selected for further analysis. Around 10% of these events have multiple B candidates. For these events, the candidate with the smallest $\chi_{\text{vtx}}^2 + \chi_{\eta'}^2$ is selected, where χ_{vtx}^2 is an estimator of the vertex quality for all charged particles not from K_S and $\chi_{\eta'}^2 = [(M(\eta') - m_{\eta'})/\sigma_{\eta'}]^2$, where $M(\eta')$ is the η' candidate mass, $m_{\eta'}$ is the nominal mass of the η' , and $\sigma_{\eta'} = 8$ MeV/ c^2 is the

width of the reconstructed η' mass. About 8% of signal MC events are reconstructed with a random photon or pion.

Several event shape variables are used to distinguish the spherical $B\bar{B}$ topology from the jetlike $e^+e^- \rightarrow q\bar{q}$ ($q = u, d, s, c$) continuum events. The thrust angle θ_T is defined as the angle between the η' momentum direction and the thrust axis formed by all particles not belonging to the reconstructed B meson. Continuum events tend to peak near $|\cos\theta_T| = 1$, while spherical events have a uniform distribution. The requirement $|\cos\theta_T| < 0.9$ is applied prior to all other event-topology selections.

Additional continuum suppression is obtained by using modified Fox-Wolfram moments [21] and $|\cos\theta_B|$, where θ_B is the angle between the flight direction of the reconstructed B candidate and the beam axis. A Fischer discriminant (\mathcal{F}) [22] is formed from a linear combination of $|\cos\theta_T|$, S_\perp [23], and five modified Fox-Wolfram moments. S_\perp is the ratio of the scalar sum of the transverse momenta of all tracks outside a 45° cone around the η' direction to the scalar sum of their total momenta. These variables are then combined to form an event-topology likelihood function \mathcal{L}_s ($\mathcal{L}_{q\bar{q}}$), where s ($q\bar{q}$) represents signal (continuum background). For channels with an $\eta' \rightarrow \rho^0 \gamma$ decay an additional variable $\theta_{\mathcal{H}}$, which is the angle between the η' momentum and the direction of one of the decay pions in the ρ^0 rest frame, is included for better signal-background separation. It behaves like a cosine (exponential) function for signal (continuum) events. We use the quality of B flavor tagging for the accompanying B meson to improve continuum rejection. The standard Belle B tagging package [24] is used, which gives the B flavor and a tagging quality r ranging from zero for no flavor identification to unity for unambiguous flavor assignment. The data are divided into three r regions. Signal-like events are selected by applying likelihood ratio $\mathcal{R} = \mathcal{L}_s/(\mathcal{L}_s + \mathcal{L}_{q\bar{q}})$ requirements optimized on Monte Carlo (MC) events in the three r regions separately, assuming either previously measured branching fractions or 5×10^{-6} .

The branching fractions are extracted using simultaneous (in ΔE and M_{bc}) extended unbinned maximum-likelihood fits for the $\eta' \rightarrow \eta \pi^+ \pi^-$ and $\eta' \rightarrow \rho^0 \gamma$ sub-decays simultaneously. The extended likelihood function used is

TABLE I. Mass windows to reconstruct intermediate states.

Mode	Mass window	(MeV/ c^2)
$\pi^0 \rightarrow \gamma\gamma$	[118, 150]	$\pm 2.5\sigma$
$\rho^0 \rightarrow \pi^+ \pi^-$	[550, 870]	—
$\eta \rightarrow \gamma\gamma$	[500, 570]	$+2.5\sigma / -3.3\sigma$
$\eta' \rightarrow \eta \pi^+ \pi^-$ (in $\eta'K$)	[945, 970]	$\pm 3.4\sigma$
$\eta' \rightarrow \rho^0 \gamma$ (in $\eta'K$)	[935, 975]	$\pm 3\sigma$
$\eta' \rightarrow \eta \pi^+ \pi^-$ (in $\eta'\pi$)	[950, 965]	$\pm 2.5\sigma$
$\eta' \rightarrow \rho^0 \gamma$ (in $\eta'\pi$)	[941, 970]	$\pm 2.5\sigma$
$K_S^0 \rightarrow \pi^+ \pi^-$	[485, 510]	$\pm 3\sigma$

$$L(N_S, N_{B_j}) = \frac{e^{-(N_S + \sum_j N_{B_j})}}{N!} \prod_{i=1}^N [N_S P_S(\Delta E_i, M_{\text{bc}_i}) + \sum_j N_{B_j} P_{B_j}(\Delta E_i, M_{\text{bc}_i})], \quad (1)$$

where N_S (N_{B_j}) is the number of signal events (background events of source j) with probability density functions (PDFs) P_S (P_{B_j}), and the index i runs over the total number of events.

The reconstruction efficiencies are determined from signal MC samples, using the EVTGEN package [25] with final state radiation simulated by the PHOTOS package [26] [thus measuring $B \rightarrow \eta/h (\gamma_{FSR})$]. The efficiencies are calculated separately for both Set I and Set II. The absolute efficiency for Set II is typically about 0.5% larger than for Set I (for efficiencies averaged over the two sets, see Table II). The signal yield is expressed as $N_S = \epsilon_1 N_{(B\bar{B})_1} \mathcal{B} + \epsilon_2 N_{(B\bar{B})_2} \mathcal{B}$, where \mathcal{B} is the signal branching fraction, and ϵ_i and $N_{(B\bar{B})_i}$ are the efficiency and the number of $B\bar{B}$ pairs for Set I and Set II. The numbers of $B^+ B^-$ and $B^0 \bar{B}^0$ pairs are assumed to be equal. Corrections due to differences between data and MC calculations are included for the charged track identification and photon, π^0 and η reconstruction, resulting in an overall correction factor of ≈ 0.9 .

The PDF shapes for each contribution are determined by MC calculations. The signal shapes for ΔE and M_{bc} are assumed to be independent. We model the signal using a Gaussian with an exponential tail (Crystal Ball function) [27] plus a Gaussian for ΔE and a Gaussian with an exponential tail for M_{bc} .

We consider four types of backgrounds separately in the fit: continuum events, $b \rightarrow c$, and two types of charmless decays. Continuum background is modeled by a first or second order polynomial for ΔE and an ARGUS function [28] for M_{bc} . Charmless B decays and $b \rightarrow c$ backgrounds are modeled with smoothed two-dimensional histograms. The contributions from charmless B decays are split into two components, one for the decay with the largest contribution and one for all other charmless decays. For $B^+ \rightarrow \eta' K^+$, the dominant mode, which is modeled separately, is $B \rightarrow \eta' K^*$; for $B^0 \rightarrow \eta' K_S^0$ it is $B \rightarrow \rho^0 K_S^0$; for $B^0 \rightarrow \eta' \pi^0$ it is $B \rightarrow \rho \rho$; and for $B^+ \rightarrow \eta' \pi^+$ it is the $B^+ \rightarrow \eta' K^+$ cross feed. The cross feed in $B^+ \rightarrow \eta' \pi^+$ is modeled with the same PDFs as used for the $\eta' K^+$ signal, shifted and with a corrected width in ΔE .

The continuum shape parameters that are allowed to float in all modes are the slopes of the polynomial and ARGUS function. The signal mean and width parameters are free for the kaon modes. For the $B^+ \rightarrow \eta' \pi^+$ mode

these parameters are fixed to the values obtained from the charged kaon mode. The resulting signal PDFs are shifted by up to -2 MeV and the width is smaller by up to 5%. For $\eta' \rightarrow \eta \pi^+ \pi^-$ modes our background MC studies show that no contributions from $b \rightarrow c$ decays are expected. The sizes of background contributions other than continuum are constrained to the values expected from the MC simulations. For example, for $B^+ \rightarrow \eta' K^+$ we expect 718 $b \rightarrow c$ events, 105 charmless events, and 10 $B \rightarrow \eta' K^*$ events. The $B^+ \rightarrow \eta' K^+$ component in the $B^+ \rightarrow \eta' \pi^+$ decay is fixed to the branching fraction of $B^+ \rightarrow \eta' K^+$ as reported here. Simultaneous fits with the branching fraction and the charge asymmetry (for the charged modes) as fit parameters are performed. The resulting projection plots are shown in Fig. 1. The reconstruction efficiencies and fit results are given in Table II.

We find first evidence for the neutral decay:

$$\mathcal{B}(B^0 \rightarrow \eta' \pi^0) = [2.79_{-0.96}^{+1.02}(\text{stat})_{-0.34}^{+0.25}(\text{syst})] \times 10^{-6},$$

and evidence for the charged decay:

$$\mathcal{B}(B^\pm \rightarrow \eta' \pi^\pm) = [1.76_{-0.62}^{+0.67}(\text{stat})_{-0.14}^{+0.15}(\text{syst})] \times 10^{-6}.$$

The ratio of the branching fractions for charged and neutral $B \rightarrow \eta' K$ decays is found to be $1.17 \pm 0.08 \pm 0.03$. The charge asymmetries for the $B^+ \rightarrow \eta' \pi^+$ and $B^+ \rightarrow \eta' K^+$ decay modes, listed in Table II, show no significant deviation from zero.

Systematic errors are estimated with various high statistics data samples. The dominant sources are the uncertainties in the reconstruction efficiency of charged tracks (3–4%), the uncertainties in the reconstruction efficiencies of η mesons and photons (3–6%), and the uncertainty of the PDF shapes and parameters (1–9%). Other systematic uncertainties arise from the K cross feed in $B^+ \rightarrow \eta' \pi^+$ ($\approx 2\%$), the differences between data and MC calculations for ΔE and M_{bc} in $B^+ \rightarrow \eta' \pi^+$ ($\approx 4\%$), the K_S reconstruction efficiency uncertainty (4%), the uncertainty of the subdecay branching fractions as given by the Particle Data Group (PDG) [29] (1.5%), the number of $B\bar{B}$ mesons produced (1%), the efficiency differences due to signal simulation by different MC generators (1.4%), the uncer-

TABLE II. Signal efficiencies (ϵ_{tot}) with subdecay branching fractions included and averaged for Set I and Set II for $\eta' \rightarrow \eta \pi^+ \pi^-$ and $\eta' \rightarrow \rho^0 \gamma$, total signal yields N_S , total number of events N_{tot} , branching fractions \mathcal{B} , charge asymmetries A_{CP} , significances σ , and goodness of fit (GOF). The first errors are statistical and the second (where given) systematic.

	$B^+ \rightarrow \eta' K^+$	$B^0 \rightarrow \eta' K^0$	$B^+ \rightarrow \eta' \pi^+$	$B^0 \rightarrow \eta' \pi^0$
$\epsilon_{\text{tot}}(\eta' \rightarrow \eta \pi^+ \pi^-)$ [%]	4.31 ± 0.03	1.19 ± 0.03	2.84 ± 0.03	1.72 ± 0.02
$\epsilon_{\text{tot}}(\eta' \rightarrow \rho^0 \gamma)$ [%]	2.78 ± 0.04	1.07 ± 0.04	2.89 ± 0.04	1.72 ± 0.03
N_S	1895.7 ± 59.5	515.3 ± 31.7	39.0 ± 13.2	35.8 ± 12.7
N_{tot}	25 281	6044	8411	1345
$\mathcal{B}[10^{-6}]$	$69.2 \pm 2.2 \pm 3.7$	$58.9_{-3.5}^{+3.6} \pm 4.3$	$1.76_{-0.62-0.14}^{+0.67+0.15}$	$2.79_{-0.96-0.34}^{+1.02+0.25}$
A_{CP}	$0.028 \pm 0.028 \pm 0.021$	—	$0.20_{-0.36}^{+0.37} \pm 0.04$	—
σ	>10	>10	3.2	3.1
(GOF)	1.1	1.5	1.2	1.4

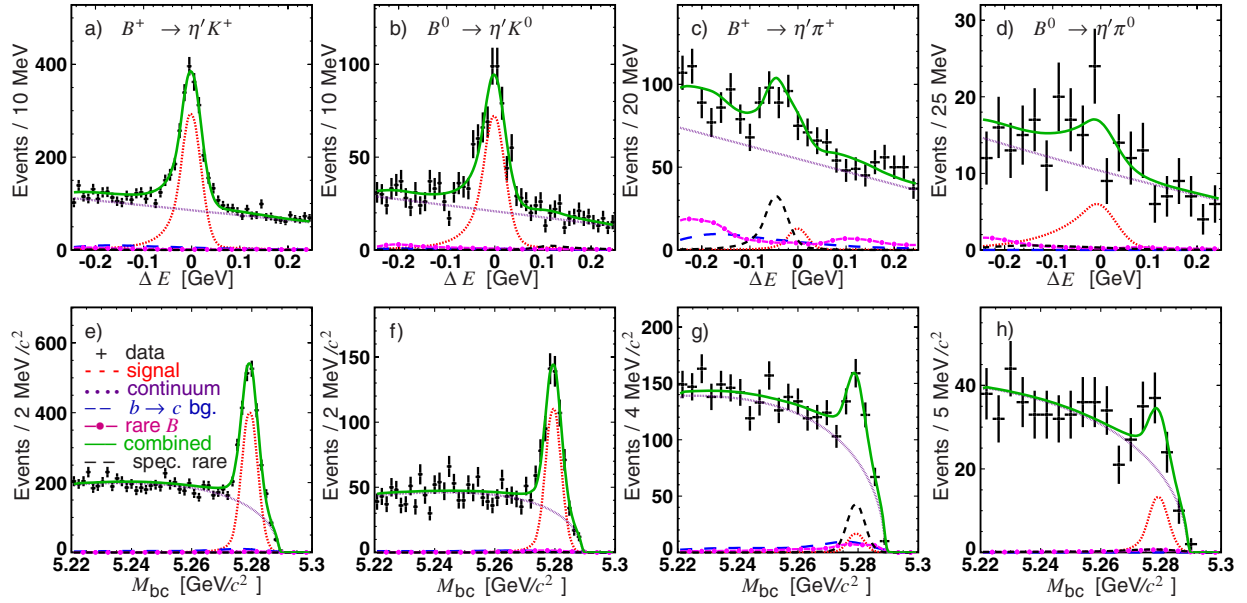


FIG. 1 (color online). ΔE and M_{bc} distributions for $B^+ \rightarrow \eta'K^+$ (a), (e), $B^0 \rightarrow \eta'K^0$ (b), (f), $B^+ \rightarrow \eta'\pi^+$ (c), (g), and $B^0 \rightarrow \eta'\pi^0$ (d), (h), respectively, for the region $M_{bc} > 5.27 \text{ GeV}/c^2$ and $-0.12 \text{ GeV} < \Delta E < 0.08 \text{ GeV}$ for $B^0 \rightarrow \eta'\pi^0$ and $-0.1 \text{ GeV} < \Delta E < 0.06 \text{ GeV}$ for all others.

tainty in the efficiency (1%) and the uncertainty from particle identification (0.7%). The systematic errors are added in quadrature and found to be $\pm 5.4\%$, $\pm 7.3\%$, $+8.5\%$, and -7.7% for $B^+ \rightarrow \eta'K^+$, $B^0 \rightarrow \eta'K^0$, $B^+ \rightarrow \eta'\pi^+$, and $B^0 \rightarrow \eta'\pi^0$, respectively. For the charge asymmetry, efficiency based systematic errors cancel. We estimate the possible detector bias on A_{CP} from the charge asymmetry of the continuum background in the $B^+ \rightarrow \eta'K^+$ sample which is obtained from the fit. We assign 0.02 as systematic error both for $B^+ \rightarrow \eta'K^+$ and $\eta'\pi^+$. Other contributions from fitting and normalization together result in a systematic error of 0.003 for $B^+ \rightarrow \eta'K^+$. For $B^+ \rightarrow \eta'\pi^+$ the uncertainties from PDF shapes and cross feed contributions add up to $^{+0.03}_{-0.04}$.

The significance of the $B^+ \rightarrow \eta'\pi^+$ yield is 3.2σ , which is calculated as $\sigma = \sqrt{2 \ln(\mathcal{L}_{\max}/\mathcal{L}_0)}$, where \mathcal{L}_{\max} and \mathcal{L}_0 denote the maximum-likelihood value and the likelihood value at zero branching fraction, respectively. The systematic error is included in the significance calculation. For $B^0 \rightarrow \eta'\pi^0$ the corresponding significance with systematics is 3.1σ .

We calculate a goodness of the fit (GOF) for ΔE and M_{bc} projections shown in Fig. 1 as a measure of the quality of the fit. The GOF is defined as the average of χ^2/dof for ΔE and M_{bc} with $\chi^2 = \sum_{i=1}^N \frac{(n_i - \nu_i)^2}{\nu_i}$, where $\nu_i(n_i)$ is number of observed (fitted) events in i th bin of total N bins and dof is a degree of freedom. The GOF values are listed in Table II.

In summary, evidence for $B \rightarrow \eta'\pi$ with greater than 3σ significance is found and improved measurements for the charged and neutral $B \rightarrow \eta'K$ decays are reported. The measurements of branching fractions for $B \rightarrow \eta'K$ decays

reported here supersede our previous results [8] and are consistent with the measurements by CLEO [7] and BABAR [6]. No charge asymmetry is observed in the decay modes $B^+ \rightarrow \eta'K^+$ and $B^+ \rightarrow \eta'\pi^+$.

We thank the KEKB group for excellent operation of the accelerator, the KEK cryogenics group for efficient solenoid operations, and the KEK computer group and the NII for valuable computing and Super-SINET network support. We acknowledge support from MEXT and JSPS (Japan); ARC and DEST (Australia); NSFC and KIP of CAS (Contract No. 10575109 and No. IHEP-U-503, China); DST (India); the BK21 program of MOEHRD, and the CHEP SRC and BR (Grant No. R01-2005-000-10089-0) programs of KOSEF (Korea); KBN (Contract No. 2P03B 01324, Poland); MIST (Russia); ARRS (Slovenia); SNSF (Switzerland); NSC and MOE (Taiwan); and DOE (USA).

- [1] Throughout this Letter, the inclusion of the charge conjugate mode decay is implied unless otherwise stated.
- [2] C. W. Chiang, M. Gronau, J. L. Rosner, and D. A. Suprun, Phys. Rev. D **70**, 034020 (2004).
- [3] Y. Grossman, Z. Ligeti, Y. Nir, and H. Quinn, Phys. Rev. D **68**, 015004 (2003).
- [4] H. K. Fu, X. G. He, and Y. K. Hsiao, Phys. Rev. D **69**, 074002 (2004).
- [5] M. Beneke and M. Neubert, Nucl. Phys. **B675**, 333 (2003).
- [6] B. Aubert *et al.* (BABAR Collaboration), Phys. Rev. Lett. **95**, 131803 (2005).
- [7] S. J. Richichi *et al.* (CLEO Collaboration), Phys. Rev. Lett. **85**, 520 (2000).

- [8] K. Abe *et al.* (Belle Collaboration), Phys. Lett. B **517**, 309 (2001).
- [9] B. Aubert *et al.* (BABAR Collaboration), Phys. Rev. Lett. **94**, 191802 (2005).
- [10] Y. Grossman and M. P. Worah, Phys. Lett. B **395**, 241 (1997).
- [11] D. Atwood and A. Soni, Phys. Lett. B **405**, 150 (1997).
- [12] W. S. Hou and B. Tseng, Phys. Rev. Lett. **80**, 434 (1998).
- [13] A. L. Kagan and A. A. Petrov, hep-ph/9707354.
- [14] A. Ali, G. Kramer, and C. D. Lu, Phys. Rev. D **58**, 094009 (1998).
- [15] D.-S. Du, C. S. Kim, and Y.-D. Yang, Phys. Lett. B **426**, 133 (1998).
- [16] S. Khalil and E. Kou, Phys. Rev. Lett. **91**, 241602 (2003).
- [17] S. Kurokawa and E. Kikutani, Nucl. Instrum. Methods Phys. Res., Sect. A **499**, 1 (2003), and other papers included in this volume.
- [18] A. Abashian *et al.* (Belle Collab.), Nucl. Instrum. Methods Phys. Res., Sect. A **479**, 117 (2002).
- [19] Y. Ushiroda (Belle SVD2 Group), Nucl. Instrum. Methods Phys. Res., Sect. A **511**, 6 (2003).
- [20] F. Fang *et al.* (Belle Collab.), Phys. Rev. Lett. **90**, 071801 (2003).
- [21] The Fox-Wolfram moments were introduced in G. C. Fox and S. Wolfram, Phys. Rev. Lett. **41**, 1581 (1978); The Fisher discriminant used by Belle, based on modified Fox-Wolfram moments (SFW), is described in K. Abe *et al.* (Belle Collaboration), Phys. Rev. Lett. **87**, 101801 (2001).
- [22] R. A. Fisher, Ann. of Eugenics **7**, 179 (1936).
- [23] R. Ammar *et al.*, Phys. Rev. Lett. **71**, 674 (1993).
- [24] H. Kakuno *et al.*, Nucl. Instrum. Methods Phys. Res., Sect. A **533**, 516 (2004).
- [25] D. J. Lange, Nucl. Instrum. Methods Phys. Res., Sect. A **462**, 152 (2001).
- [26] E. Barberio and Z. Was, Comput. Phys. Commun. **79**, 291 (1994).
- [27] J. E. Gaiser *et al.* (Crystal Ball Collaboration), Phys. Rev. D **34**, 711 (1986).
- [28] H. Albrecht *et al.* (ARGUS Collaboration), Phys. Lett. B **241**, 278 (1990).
- [29] S. Eidelman *et al.* (Particle Data Group), Phys. Lett. B **592**, 1 (2004).